Tracking and Control of a Small Unmanned Aerial Vehicle using a Ground-Based 3D Laser Scanner

Ryan Arya Pratama and Akihisa Ohya

Abstract— **In this work, we describe a method to measure the position and orientation of a small unmanned aerial vehicle (UAV) using a ground-based 3D laser scanner. A method to calculate UAV position from laser scanner data with weighted averaging is presented. In complement, a method to calculate UAV orientation using laser intensity data is proposed. High intensity points needed for the method is facilitated by installation of three reflective stripes on three corners of the UAV's propeller guard. Lastly, results from early experiments on controlling the UAV using the position measurement calculated from the laser data is presented.**

I. INTRODUCTION

Effective navigation of air robots requires good localization and path planning. However, there is a limit to how much payload an air robot can carry, including sensing payloads. While GPS navigation is workable in areas where it is available, there are many cases where one would like to operate an air robot in GPS-denied environments, such as in dense urban settings or inside buildings.

Furthermore, small movements during hover (in case of helicopters or quadrotors) or high-speed movement (in-case of fixed-wing aircrafts) make compensating sensor data for self-movement more difficult. Both the payload problem and the data processing problem are made worse the smaller the air robot is, as it is only capable of carrying fewer sensors, and high-frequency self-movements are worse.

By using a ground robot to assist the air robot with localization and path planning, we can reduce the sensing and computing requirement on-board the air robot. The resources freed up by this may then be used for added functionality or agility for the air robot, such as a specialized sensor, or specialized tool to work on objects placed high above ground, such as the top of a pole or a ceiling fixture.

Ground tracking of air robot also widens the potential for obstacle avoidance behaviour of the air robot, especially for obstacles that are not reflected in the map (when a map is available) or moving obstacles. As all sensors used for localization of the air robot is placed on the ground robot, there are fewer restrictions on their weights and sizes. Therefore, the sensor configuration can be optimized for performance in obstacle detection instead of manoeuvrability of the air robot.

Ryan A. P is a PhD student at Department of Computer Science, Graduate School of Systems and Information Engineering, University of Tsukuba, Japan ryan-p@roboken.cs.tsukuba.ac.jp

A. Ohya is professor at Department of Computer Science, Graduate School of Systems and Information Engineering, University of Tsukuba, Japan ohya@cs.tsukuba.ac.jp

A stationary base station, or a fixed vision system may work well for a fixed working area, but using a mobile ground robot expands the working area of the whole system to anywhere the mobile robot can navigate. With this configuration, it is possible to expand the operating area of the air robot from within a specialized room with a fixed vision system to a whole building or complex of buildings, or to wide areas outdoors. Moreover, the mobility of the ground robot prevents prolonged occlusion of the vision system that may fail the tracking; the mobile robot can move to a better vantage point. This will be important in working areas with obstacles, especially moving ones, that may occlude the line-of-sight from the mobile robot to the air robot.

In this work, we attempt to tackle tracking and control of an air robot using a ground-based 3D laser scanner. At this stage the laser scanner is stationary. Expansion to a mobile ground robot is planned as a future work.

This document shall be structured in the following way: first, an overview of related works shall be presented. Following that, the method used to track the position and orientation of the flying robot will be described. Next, results from early experiments in controlling the air robot using the tracking data will be shown. Finally a conclusion will close the document.

II. RELATED WORKS

There are past researches on tracking air robots from a fixed sensing platform, either with cameras or laser scanners. There are also past researches on tracking moving objects from ground mobile robots. However, the tracked objects are on the ground and do not communicate with the mobile robot. Research on cooperation between ground and air robots outlined in Section I is relatively sparse and would prove to be valuable to researches on cooperation between robots.

Cooperation between air and ground robots have been explored in previous works. In [1], the task of controlling a formation of ground robots using an air robot was explored. Ground-air cooperation in rescue operation in indoor, GPS-denied environment was explored in [2]. In the paper, the air robots are equipped with cameras and act as scouts that explore the operating area for rescue targets, based on the condition of the target, the control station decides which ground robot to send and its task. Ground-air cooperation for situational awareness and urban surveillance was explored in [3]. There, in addition to map-building by the air robots, the ground robots build a map of wireless signal strength, which is used to maintain communication between the robots

throughout the mission. An example mission of finding and tracking a uniformed person was described in the paper.

Tracking of air robot with a 3D laser scanner on a fixed platform was attempted in [4]. The paper used manually controlled mini-helicopter and did not include obstacle avoidance.

On the front of object tracking from mobile robot, [5] describes a method of tracking multiple moving objects using adaptive particle filter using a single camera. The paper describes a method to compensate robot movement in comparing images for several types of robots: a helicopter, a self-balancing robot, and a statically-stable mobile robot. The work may be adapted for tracking of air robot and moving obstacles. Ways to adapt the sensing model to use 3D laser scanner in place of/in addition of the camera may be investigated.

Air robot navigation using only sensors mounted on the air robot, in this case a monocular camera, is described in [6]. However, even in this case, the camera image is transmitted into a computer which is not carried by the flying robot. This then limits the operation area to the communication range between the data processing computer and the air robot.

A similar work using a pair of air and ground robot was carried out in [7]. In their research, they installed infrared LEDs as markers on the flying robot and used them to track the position and pose of the air robot from a ground robot.

III. HARDWARE PLATFORM

A. Air Robot

The air robot used in this work is Parrot's AR.Drone 1.0, a commercially available quadcopter unmanned aerial vehicle. Henceforth it will simply be called the drone. It is equipped with several sensors: a forward facing camera, a downward facing camera, an inertial measurement unit, and an ultrasound sensor pointing downward to measure altitude. Pictures of the drone are shown in Figs. 5a and 5b.

Communication to the drone is done through wireless LAN. By default, the drone creates its own access point to which a computer may connect, but it is possible to make it connect to a pre-defined access point so that devices other than the drone and its controlling computer can share the network. In this work, the drone, a computer, and the laser scanner all connect to the same network.

Drone speed control is done by its onboard controller and a user communicating to it via its driver needs only to give speed references in x, y, and z directions along with yaw speed reference. We use the ardrone_autonomy[8] ROS package as driver.

B. Laser Scanner

The sensor we used is a 3D laser scanner built from a planar laser scanner by mounting it on a rotating platform (Fig. 2). Laser scanner was chosen for its point density and the availability of light intensity measurement, which is important for the orientation measurement method we will describe in Section IV-B.

The planar laser scanner scans the environment and outputs distance and light intensity data at a nominal rate of 40 Hz. Each scan returns up to 1081 distance points at 0.24°resolution. It is mounted on a rotating platform which rotates at 0.5 rotation per second while regularly outputting a planar slice of laser scan (see Fig. 1a for an illustration of a planar scan). After the platform has completed half a rotation, we can assemble a frame covering the full 360° around the laser scanner (Illustrated in Fig. 1b).

If we do not allow any scan overlap between successive frames, we get one frame every second. In our experiments, we let consecutive frames overlap with each other such that frames are output at 10 Hz, i.e., every 100 ms, the scans from the latest half rotation are assembled into a frame.

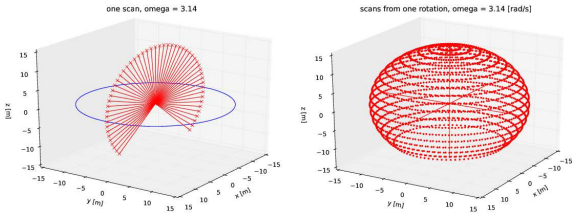

(a) (b)

Fig. 1. Illustration of one scan from the laser scanner (a) and from one frame assembled from several scans (b)

The farther away the target object is from the laser scanner, the fewer planar scans may intersect it, and in turn the fewer points we get on it, and consequently the lesser detail we can get from the measurement. Our target object—the drone—has a bounding dimensions of approximately $0.53 \times 0.53 \times 0.10$ m. Figs. 3a and 3b show how laser measurements of the drone look like directly above the

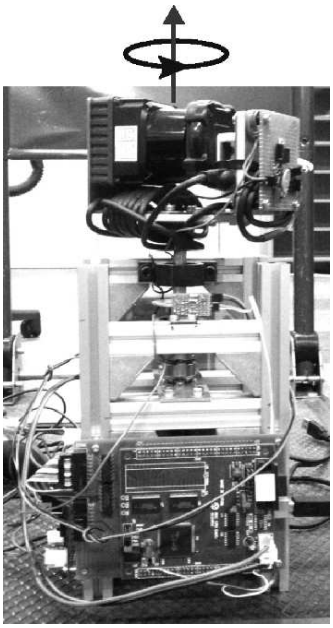

Fig. 2. Picture of the 3D laser scanner with its axis and direction of rotation (counter-clockwise) marked

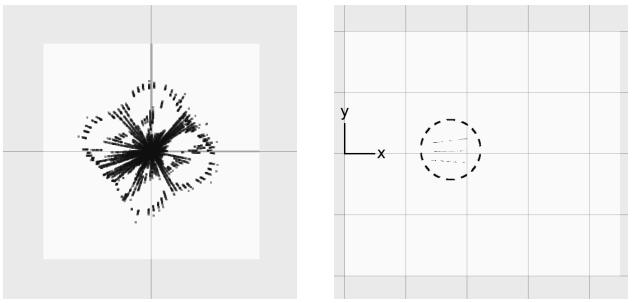

(a) (b)

Fig. 3. Laser points on the drone when it is directly above the sensor (a) and at 1.5 m away from the sensor (within dashed circle) (b). White box in (a) is 1×1 m, grid in (b) is 1 m to each side

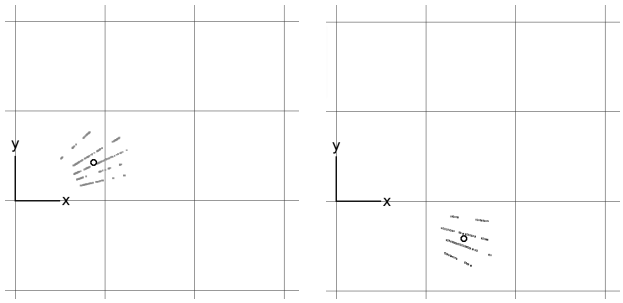

(a) (b)

Fig. 4. Examples of position measurement by averaging at two different positions relative to the sensor. Grid is 1 x 1 meter. Estimated position is marked by a white circle

sensor and at approximately 1.5 m away from it. Naturally, the condition becomes more challenging when the target is moving.

Our target condition is to have the drone fly within 2 m from the laser scanner with speed of at most 0.5 m/s.

IV. DRONE TRACKING

A. Position Measurement

At this stage of the research, we do not employ a special algorithm to separate points on the drone from points on the environment. We simply do our experiment in an open space and designate a volume in it as the region of interest; all point data in that region are then assumed to lie on the target object. In our experiments, a volume of $3 \times 3 \times 3$ m in front of the laser scanner was used. Future work will look into extending the operation into less simplistic conditions.

As all points in the region of interest are assumed to lie on the drone, we can calculate its location by taking an average of all points. Naturally, we get more points nearer the laser scanner, so if we assign the same weight to all points, the output of the averaging will be biased towards the origin, i.e. the calculated location will be closer to the origin than it actually is. To lessen this bias, we can introduce weighting to the averaging. In this case, the distance from each point to the laser scanner is used as the weight.

First, let us denote the laser scanner coordinate system as L, with its z-axis along the rotation axis of the rotating platform of the laser scanner and its x-axis pointing straight ahead. Given a set of point P of distance measurement from the laser scanner, expressed in the coordinate system of the laser scanner, we can then calculate the drone location ${}^{L}x_{drone}$ with:

$$ {}^{L}x_{drone} = \frac{1}{\sum_{i=1}^{N} w_i} \sum_{i=1}^{N} w_i {}^{L}p_i \quad {}^{L}p_i \in P \qquad (1) $$

This calculation is done every time we get a new frame from the laser scanner: every 100 ms.

Examples of position measurement result are shown in Fig. 4a and 4b.

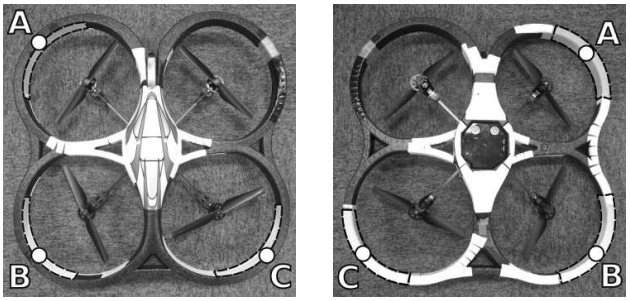

(a) (b)

Fig. 5. Location of reflective markers (dashed outline) on the drone. Top view (a) and bottom view (b)

B. Orientation Measurement

With the symmetric shape of the drone, we cannot get its orientation simply by looking at the shape of the point cloud output by the laser scanner. In order to facilitate orientation measurement, three reflective stripes were placed on three corners of the drone's propeller guard. The configuration is as shown in Figs. 5a and 5b. These locations were chosen to make the drone appear asymmetrical to the sensor, so we would be able to calculate its orientation. Laser beams reflected by these stripes result in points with higher intensity, which can be easily distinguished from the remaining low-intensity points on the drone.

To calculate drone orientation, first we divide the points into high intensity and lower intensity point clouds. This is done by clustering the points by intensity into two clusters whose centroids are intialized at the highest intensity point and the lowest intensity point; standard k-means algorithm is used. Iteration is stopped when the sum of absolute distances from each point to its corresponding centroid has stopped getting smaller between iteration or when ten iterations have been done.

The high intensity points are then spatially clustered into three clusters, with each cluster represented by its center point. The three center points from the three clusters correspond to the three corners on the drone with the reflective stripes.

Let us call these points A, B, and C according to Fig. 6. The positions of points A, B, and C relative to the origin of the laser scanner are ${}^{L}p_A$, ${}^{L}p_B$, and ${}^{L}p_C$. The orientation

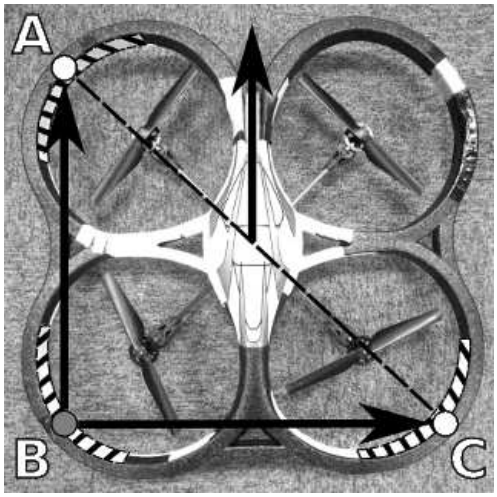

Fig. 6. Points A, B, and C on the reflective stripes on the drone. Drone position is midway between A and C, and drone orientation is along BA

of the drone is then along the line from B to A, or:

$$r = {}^{L}p_A - {}^{L}p_B \tag{2}$$

Let us call the components of r along the x, y, z axes as r_x, r_y, r_z, or $r = \begin{bmatrix} r_x \\ r_y \\ r_z \end{bmatrix}$. The orientation of the drone in terms of yaw angle is then:

$$\theta_{\mathtt{yaw}} = \arctan\left(\frac{r_y}{r_x}\right) \tag{3}$$

Having three high intensity clusters, we can then begin finding correspondence between the three clusters with A, B, and C.

First, let us represent each high intensity cluster by its center, replacing the many points of each cluster with a single point that is their average. Then, observing that line AB is orthogonal to line BC, we can find B by finding the combination that results in the lowest $\cos \angle ABC$. The three possible correspondences are shown in Fig. 7.

We are then left with two choices for A and B, as shown in Fig. 8. Next, we make the assumption that the drone is never upside-down. We then choose A and B such that $BC \times BA$ points to positive z axis in the laser scanner's frame of reference. This is practical as the current setup of the drone cuts off its power when it is tilted too much; there will not be a case where the laser scanner sees the drone flying upside-down.

An example of a successful orientation measurement result is shown in Fig. IV-B.

From experiments, we found that this method has several common failure modes such as those shown in Figs. 10a and 10b. We think that the following are the possible causes: when the drone is moving, there is a chance that the position of the three corners are distorted; when the drone is far away there is a chance that one or more of the corners are not seen by the sensor. In such cases, the position and orientation data from this method cannot be used and must be rejected. We

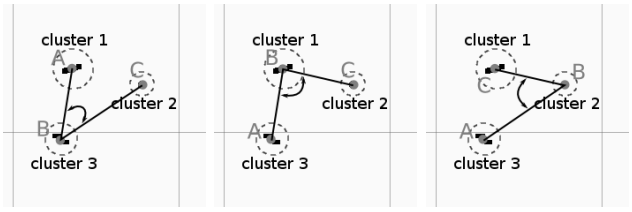

(a) (b) (c)

Fig. 7. Three possible choices for correspondence between the three high-intensity clusters and points A, B, and C. Combination that results in $\angle ABC$ nearest to 90°, or lowest $\cos \angle ABC$, tells us which cluster corresponds to B (in this case the combination in (b))

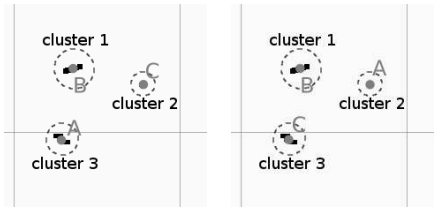

(a) (b)

Fig. 8. Two possible choices for A and C when we have found B. The combination that results in $BA \times BC$ pointing in positive z-axis in the laser scanner frame of reference is taken as the correct combination. With the positive z-axis pointing out of the paper plane, the combination in (a) is picked.

use these criteria to screen the output of this method to reject bad cases:

orthogonality
: BA and BC must be nearly orthogonal. This is tested by checking the value of the cosine of the angle between BA and BC:

$$\cos(90° + \epsilon) < \frac{BA \cdot BC}{|BA||BC|} < \cos(90° - \epsilon) \tag{4}$$

with ϵ being a small tolerance value.

length similarity
: BA and BC must have similar length. This is tested by checking the ratio between the lengths of the two vectors:

$$1 - \alpha < \frac{|BA|}{|BC|} < 1 + \alpha \tag{5}$$

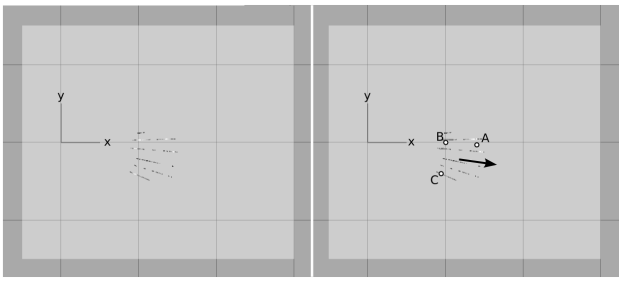

Fig. 9. Orientation measurement result example. Raw point data on the right, measurement result on the left. Lighter points have higher intensity. The orientation is along the arrow and points A, B, and C are as labelled. Grid is 1 m to its side

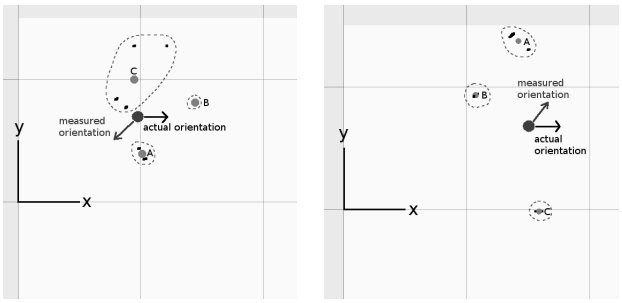

(a) (b)

Fig. 10. Examples of cases when the ABC point methods for orientation measurement fails. Points from a moving drone were measured so that points in cluster C were too far apart (a), clusters B and C are too far apart (b). In both cases, the drone was actually facing straight to the right ($+x$ direction)

α is a small tolerance value.

actual dimension

Finally, the lengths of BA and BC must closely match those of the actual drone. If the side of the drone is of length d, then

$$d - \delta < |BA| < d + \delta \tag{6}$$

again, δ is a small tolerance.

With these screening criteria in place, we found that unless the drone is hovering or moving very slowly, it is very difficult to get a good (not rejected) orientation measurement with this method. The non-regularity of this method makes it unsuitable for control. To control the drone, we combine this method with the previously described weighted average position measurement. As drone orientation does not change easily, intermittent measurement resulting from this method can still be used, by assuming that drone orientation does not change between good orientation measurements.

C. Measurement Result

We tested this method by measuring the position and orientation of a hovering drone. The drone was controlled with proportional control to keep its hover position at $(x, y, z) = (1.5,\ -0.7,\ 2.0)$ m relative to the laser scanner. Hover set point is the first drone position measured by the laser scanner after takeoff.

The region of interest for position and orientation measurement is a $3 \times 3 \times 3$ m box, with ranges from 0 to 3 m along x-axis, -1.5 to 1.5 m along y-axis, and 1 to 4 m along z-axis, with the origin on the laser scanner.

The measurement results are as shown in Fig. 11. Notice the intermittent measurement of the drone orientation.

In another experiment, precision of the position measurement is compared to distance markers on the floor ((x, y) only). From this evaluation, we find that the x, y position measurement from laser data is within approximately 400 mm of floor-marker measurement. Part of the discrepancy is from the imprecision of the floor-marker measurement. Several points showing the difference between position measurements by laser scanner and by floor-marking are shown in Table I.

TABLE I

EXAMPLE POINTS FROM LASER AND FLOOR-MARKER POSITION

Laser position $(x,\ y)$ m	Floor-marker position $(x,\ y)$ m
$(0.62,\ 1.15)$	$(1.08,\ 0.92)$
$(0.78,\ 1.05)$	$(1.08,\ 0.78)$
$(1.10,\ 0.88)$	$(1.25,\ 0.65)$

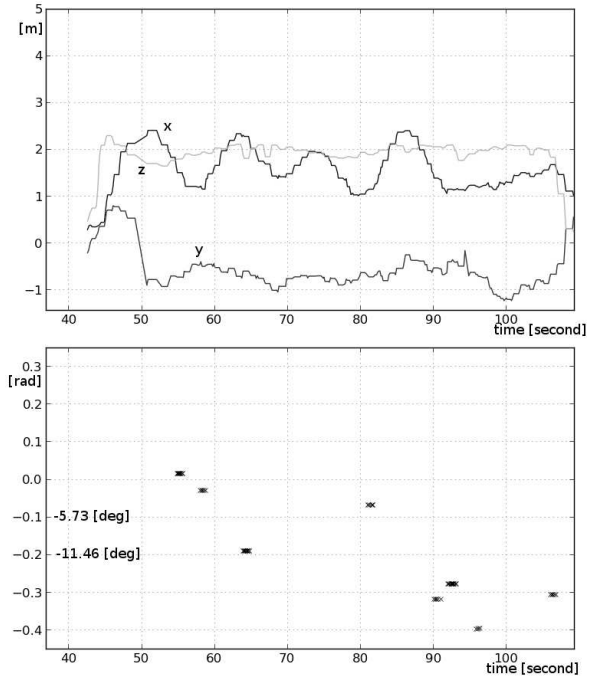

Fig. 11. Result from position and orientation measurement experiment. Drone was controlled to hover at $(x, y, z) = (1.5, -0.7, 2.0)$ m relative to the laser scanner with a proportional controller. Orbiting behaviour around the setpoint was observed. Notice the intermittent measurement of drone orientation.

From this result, we see that we can measure a flying drone's position and orientation and use the measurement to make it orbit a setpoint using laser data and the method described in Sections IV-A and IV-B.

V. DRONE CONTROL

Some limited experiments have been done on drone control using the position and orientation data obtained from the methods described in Section IV-B. The experiment was limited in these ways:

- The drone was initialized to a known yaw angle: $0°$
- Only the x and y positions were controlled; altitude was not actively maintained beyond the initial takeoff. Specifically, the reference for z velocity is always set to zero.

Drone position was controlled with a proportional controller which block diagram is shown in Fig. 12. Speed references $\left[\begin{smallmatrix} u_x \\ u_y \end{smallmatrix}\right]$ are calculated as follows:

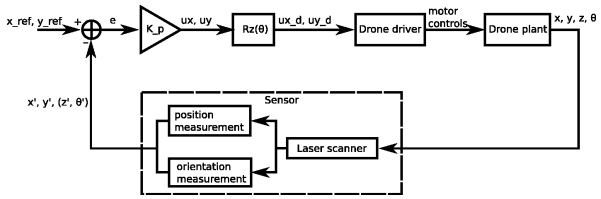

Fig. 12. Control system block diagram. $Rz(\theta)$ transforms the speed references from laser scanner frame to drone frame. The latest known drone yaw angle is used for coordinate transformation, with zero used at initialization

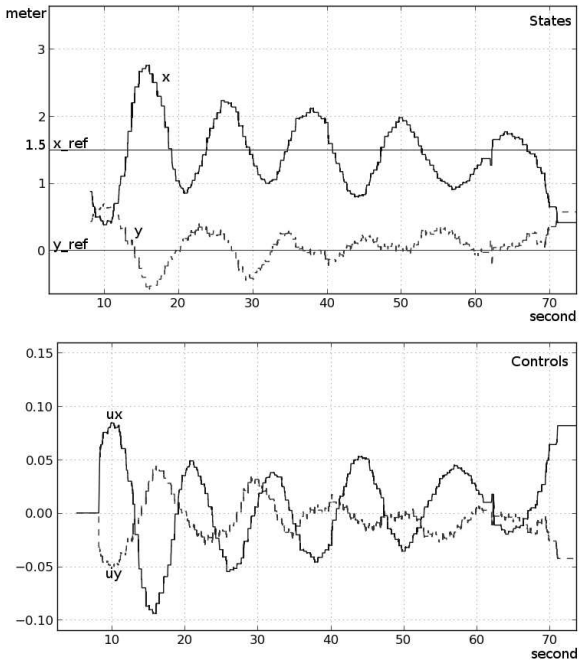

Fig. 13. Drone states (top) and control inputs (bottom) for xy-control. With setpoints $x_{ref} = 1.5$ and $y_{ref} = 0.0$. Only proportional control was used. The drone orbited around the setpoint until it is commanded to land near the 70 s point.

$$e_x = x_{ref} - x \tag{7}$$

$$e_y = y_{ref} - y \tag{8}$$

$$\begin{bmatrix} u_x \\ u_y \end{bmatrix} = R_z(\theta) K \begin{bmatrix} e_x \\ e_y \end{bmatrix} \tag{9}$$

With $R_z(\theta)$ transforming the speed references from sensor frame to drone frame.

Setpoint used was $(x_{ref}, y_{ref}) = (1.5, 0.0)$. We see in Fig. 13 that we were able to control the drone to orbit in a circle around the setpoint. In this experiment, the drone did not converge to its setpoint before it was commanded to land near the 70 s point. Further tuning of the controller may reduce the oscillation, and make the drone hover over the setpoint.

VI. CONCLUSION AND FUTURE WORK

We have presented in this work a method to track the position and orientation of a small unmanned aerial vehicle—a drone—from a ground-based 3D laser scanner. Environment and drone data was separated by simply setting a region of interest within the experiment area and assuming all data inside the region of interest to lie on the drone.

Drone position was calculated by a weighted average of all laser points on the drone, with the weight being the distance of each point to the laser scanner origin. Drone orientation measurement was facilitated by adding three patches of reflective stripes on three corners of the drone's propeller guard. By segmenting out and clustering high intensity points from points lying on the reflective stripes, we were able to get the position and orientation of the drone. Drone movement and distance affect this method adversely and several screening criteria based on the actual dimension of the drone had to be done. As a result, a considerable amount of the orientation calculation output must be rejected.

Future work will expand drone control to let us control drone orientation and to give the drone more than one setpoints, i.e., to let the drone move from place to place instead of just maintaining its hovering position. Further we will also expand the research by installing the laser scanner on a mobile ground robot and move it together with the drone. Then, we will relax the requirement of an empty region-of-interest to let the ground-air pair operate in more realistic environments. Fusing laser data with other sensors, such as the drone's on-board IMU will also be investigated.

VII. ACKNOWLEDGMENTS

We would like to thank Dr. Shigeru Bando for his suggestion and advice on the usage of reflective stripes for orientation measurement

REFERENCES

[1] N. Michael, J. Fink, and V. Kumar, "Controlling a team of ground robots via an aerial robot," in *Intelligent Robots and Systems, 2007. IROS 2007. IEEE/RSJ International Conference on*, pp. 965–970, IEEE, 2007.

[2] C. Luo, A. P. Espinosa, A. De Gloria, and R. Sgherri, "Air-ground multi-agent robot team coordination," in *Robotics and Automation (ICRA), 2011 IEEE International Conference on*, pp. 6588–6591, IEEE, 2011.

[3] M. A. Hsieh, A. Cowley, J. F. Keller, L. Chaimowicz, B. Grocholsky, V. Kumar, C. J. Taylor, Y. Endo, R. C. Arkin, B. Jung, *et al.*, "Adaptive teams of autonomous aerial and ground robots for situational awareness," *Journal of Field Robotics*, vol. 24, no. 11-12, pp. 991–1014, 2007.

[4] J. Martínez, A. Pequeno-Boter, A. Mandow, A. García-Cerezo, and J. Morales, "Progress in mini-helicopter tracking with a 3D laser rangefinder," in *World Congress*, vol. 16, pp. 1377–1377, 2005.

[5] B. Jung and G. S. Sukhatme, "Real-time motion tracking from a mobile robot," *International Journal of Social Robotics*, vol. 2, no. 1, pp. 63–78, 2010.

[6] J. Engel, J. Sturm, and D. Cremers, "Camera-based navigation of a low-cost quadrocopter," in *Proc. of the International Conference on Intelligent Robot Systems (IROS)*, Oct. 2012.

[7] M. Faessler, E. Mueggler, K. Schwabe, and D. Scaramuzza, "A monocular pose estimation system based on infrared leds," in *IEEE International Conference on Robotics and Automation (ICRA), Hong Kong*, 2014.

[8] "ardrone_autonomy github page." `https://github.com/AutonomyLab/ardrone_autonomy`. Accessed: 2014-07-28.